General Disclaimer

One or more of the Following Statements may affect this Document

- This document has been reproduced from the best copy furnished by the organizational source. It is being released in the interest of making available as much information as possible.

- This document may contain data, which exceeds the sheet parameters. It was furnished in this condition by the organizational source and is the best copy available.

- This document may contain tone-on-tone or color graphs, charts and/or pictures, which have been reproduced in black and white.

- This document is paginated as submitted by the original source.

- Portions of this document are not fully legible due to the historical nature of some of the material. However, it is the best reproduction available from the original submission.

NASA TECHNICAL MEMORANDUM

NASA TM X- 74002

NASA TM X- 74002

THE FLOW FIELD OF AN UNDEREXPANDED H_2 JET COAXIALLY INJECTED INTO A HOT FREE OR DUCTED SUPERSONIC JET OF AIR OR NITROGEN

Renaldo V. Jenkins

NATIONAL AERONAUTICS AND SPACE ADMINISTRATION
LANGLEY RESEARCH CENTER, HAMPTON, VIRGINIA 23665

February 1977

1. Report No. NASA TM X-74002	2. Government Accession No.	3. Recipient's Catalog No.
4. Title and Subtitle THE FLOW FIELD OF AN UNDEREXPANDED H_2 JET COAXIALLY INJECTED INTO A HOT FREE OR DUCTED SUPERSONIC JET OF AIR OR NITROGEN		5. Report Date February 1977 6. Performing Organization Code 37.440
7. Author(s) Renaldo V. Jenkins		8. Performing Organization Report No.
9. Performing Organization Name and Address NASA Langley Research Center Hampton, VA 23665		10. Work Unit No. 505-05-41-07 11. Contract or Grant No.
12. Sponsoring Agency Name and Address National Aeronautics and Space Administration Washington, D.C. 20546		13. Type of Report and Period Covered Technical Memorandum 14. Sponsoring Agency Code

15. Supplementary Notes

This is the final release of special information not suitable for formal publication which serves the following need: disseminates new information to those in industry and government agencies in referenceable form.

16. Abstract

This report presents experimental data obtained in an investigation of the mixing of an underexpanded hydrogen jet in a supersonic flow both with and without combustion. Tests were conducted in a Mach 2 test stream with both air and nitrogen as test media. Total temperature of the test stream was 2170 K and static exit pressure was about one atmosphere. The static pressure at the exit of the hydrogen injector's Mach 2 nozzle was about two atmospheres.

Primary measurements included shadowgraphs and pitot pressure surveys of the flow field. Pitot surveys and wall static pressures were measured for the case where the entire flow was shrouded. The results are compared to similar experimental data and theoretical predictions for the matched pressure case.

17. Key Words (Suggested by Author(s))	18. Distribution Statement
Aircraft Propulsion and Power Supersonic Combustion Underexpanded H_2 Jet Hypersonic Propulsion	Unclassified - Unlimited

19. Security Classif. (of this report)	20. Security Classif. (of this page)	21. No. of Pages	22. Price*
Unclassified	Unclassified	33	$4.00

*For sale by the National Technical Information Service, Springfield, Virginia 22161

THE FLOW FIELD OF AN UNDEREXPANDED H_2 JET COAXIALLY INJECTED INTO A HOT FREE OR DUCTED SUPERSONIC JET OF AIR OR NITROGEN

Renaldo V. Jenkins

Langley Research Center

SUMMARY

This report presents experimental data obtained in an investigation of the mixing of an underexpanded hydrogen jet in a supersonic flow both with and without combustion. Tests were conducted in a Mach 2 test stream with both air and nitrogen as test media. Total temperature of the test stream was 2170 K and static exit pressure was about one atmosphere. The static pressure at the exit of the hydrogen injector's Mach 2 nozzle was about two atmospheres. The data obtained consisted of shadowgraphs and radial pitot pressure profiles for the free-jet case, duct wall static pressures, and radial pitot pressure profiles for the ducted case. The radial pitot profiles for the ducted case were taken at the end of ducts of four different lengths.

Comparison of the reacting and nonreacting results shows that combustion alters the flow field pitot pressure distribution from that of the nonreacting flow. These differences in pressure distribution are particularly noticeable at large downstream locations. The longest ducted combustion case produces a near-centerline region of low pitot pressure with an external region of constant pressure. On the other hand, the nonreacting case has a nearly constant pitot pressure across the entire field.

The large difference in centerline total pressure between the underexpanded and previously tested, fully expanded injector at the jet exit rapidly diminished so that at about 20 jet radii, differences between the two sets of data were less than 12 percent. Profiles of the underexpanded and fully expanded jets were similar at large downstream distances; however, a jet asymmetry problem existed in the present underexpanded jet profiles which was probably caused by a small extraneous shock generated in the facility nozzle.

INTRODUCTION

The supersonic combustion ramjet (scramjet), using hydrogen fuel, looms as a key component for a major advance in aircraft technology. References 1 through 4 discuss the technological status of hypersonic airbreathing aircraft with hydrogen-burning scramjets and point out advantages including the large

heat-sink capacity of liquid hydrogen fuel. This high heat-sink feature furnishes the potential for cooling the engine and aircraft.

At NASA Langley Research Center, there is a multi-faceted research effort directed toward providing technology for hydrogen-burning scramjets. In the past this effort involved a variable-geometry axisymmetric engine which had a translating centerbody. Presently, however, this effort is focused on a fixed-geometry type of configuration which can be integrated into the aircraft design. With the integrated design, the aircraft forward and aft body surfaces are used in processing the flow to and from the engine. The various facets of the total research effort include inlet and nozzle research (refs. 5 through 8), turbulent heat transfer (ref. 9), basic combustion and mixing research (refs. 10 through 14), parametric investigation of combustor geometry, subscale engine tests, and research on structural and cooling concepts (refs. 15 and 16).

Basic combustion and mixing research is necessary if reliable heat release predictions through the combustor are to be accomplished. Understanding the basic combustion processes and the resulting heat release should lead to the ability to design a combustor with high performance and low cooling. Considerable research has been accomplished studying the parallel injection of a supersonic flow of hydrogen into a supersonic test stream for the case where static pressures of the two streams are matched. (See refs. 10 through 12.) However, for the case with the hydrogen jet underexpanded (H_2 static pressure greater than the supersonic test stream) there has been relatively little research. The theoretical treatment of this case is complex because of the shock-viscous layer interaction. Recently the theory for the underexpanded jet has been pursued to some extent (refs. 17 and 18), and when coupled with appropriate experimental research, the combustion and mixing of the underexpanded jet should be better understood. In any application of the scramjet engine design with supersonic injection, underexpanded injection will be encountered if the engine operates over a range of altitude, Mach number, and fuel equivalence ratio.

The present investigation consists of a study of an underexpanded hydrogen jet exhausting into a heated supersonic flow of air or nitrogen. The air-hydrogen mixture provided a reacting flow and the nitrogen-hydrogen mixture provided a nonreacting flow. Primary measurements included shadowgraphs and pitot pressure surveys of the flow field. Pitot surveys and wall static pressures were measured for the cases where the entire flow was shrouded. The results are compared to similar experimental data and theoretical predictions for the matched pressure case.

SYMBOLS

$\dot{m}_{air}$	air mass flow rate
$\dot{m}_{H_2}$	hydrogen mass flow rate
$\dot{m}_{N_2}$	nitrogen mass flow

p	static pressure (measured along duct wall)
p_j	jet static pressure
p_∞	test stream static pressure
p_{t_0}	test stream vessel stagnation pressure
p_{t_2}	pitot pressure (measured)
r_j	jet radius at exit of injector (0.3175 cm)
x	nondimensional coordinate along the jet axis
y	nondimensional coordinate normal to the jet axis
ϕ	equivalence ratio; the ratio of the actual $\dot{m}_{H_2}$ to that required for stoichiometric reaction, $\frac{\dot{m}_{H_2}}{0.02915\ \dot{m}_{air}}$ (the fictitious ϕ's for nitrogen test medium are computed as if the test stream were air $\frac{\dot{m}_{H_2}}{0.02915\ \dot{m}_{N_2}}$:)
$\Delta\lambda$	Kawamura parameter - Equation 1

APPARATUS AND INSTRUMENTATION

Facility and Test Conditions

The experiment was conducted in the Langley Ceramic-Heated Tunnel. This facility, described in reference 19, has a bed of zirconia pebbles which is heated by the combustion products from a propane burner. The hot test gas is obtained by passing the test medium (air or nitrogen) through the heated pebbles. In this manner, test gas total temperatures up to 2530 K can be furnished with a maximum stagnation pressure of 4 MN/m^2.

A schematic of the test apparatus is given in figure 1. A Mach 2 hydrogen injector is centered in and extends 0.318 cm downstream of the exit of the facility Mach 2 nozzle. Measurements were obtained in the free-jet mode and ducted mode. The free-jet mode configuration is obtained by removing the constant area duct extending from plane A-A to plane B-B of figure 1. Tests

were conducted with both air and nitrogen as test media. For all tests, the total temperature of the test stream was 2170 K with a nozzle exit (static) temperature of approximately 1340 K. The stagnation pressure ranged from 0.774 to 0.858 MN/m^2, resulting in test gas flow rates of 1.23 to 1.39 kg/sec and nozzle exit (static) pressures of 0.101 to 0.112 MN/m^2.

Hydrogen Injector

The hydrogen injector, which is mounted coaxially with the main nozzle, is a 0.953 cm (3/8 in.) stainless steel tube with a 5° conical Mach 2 nozzle. This H_2 injector diameter is 0.635 cm at the exit and 0.488 cm at the throat. The injector exit lip thickness is 0.159 cm. The cooling needed to protect the injector during each test is provided by the injectant (hydrogen).

In the present tests the hydrogen, supplied at ambient temperature, was heated to a total temperature of approximately 470 K as it cooled the injector. Hydrogen was injected at stagnation pressures that ranged from 1.59 to 1.94 MN/m^2 producing mass flow rates of 0.015 to 0.018 kg/sec. Based on the total flow in the facility nozzle, these hydrogen flow rates resulted in equivalence ratios that varied from 0.381 to 0.467. The exit static pressures were from 0.203 to 0.248 MN/m^2. The injector exit pressure was therefore about 2 times the test stream static pressure for these tests.

Circular Combustors

In the ducted mode, constant area ducts of four different lengths (9.53, 12.70, 30.48, and 45.72 cm) were individually attached to the facility nozzle to form circular combustors. These combustors, constructed of stainless steel, are uncooled (heat sink) and have static pressure orifices arranged in three rows (designated P, Q, and R in figure 2) that run axially along the duct with each row spaced 120° apart. A schematic of the 12.7 cm combustor accompanied by a table summarizing the orifice locations for all four ducts is given in figure 2.

Pitot Probes

Two different pitot probe designs were used in the present tests. One design is a modified version of a probe developed by the Applied Physics Laboratory of Johns Hopkins University and reported in reference 13. This design is illustrated in figure 3. It has an outside diameter of 0.635 cm and a tip half-angle of 30°. The other design is a slightly modified version of a Langley Research Center probe described in reference 14. As illustrated in figure 4, it has an outside diameter of 0.914 cm and a tip half-angle of 20°.

Probes of both designs are water cooled by a no return method. In this method, water is supplied through a single passage in the main body of the probe, sprayed against the rear of the probe tip, and then injected into the test stream at a location behind the pressure sensing region. Once in the test stream, the water is swept downstream over the probe body furnishing further

cooling.

In the case of the APL probe design (fig. 3), the cooling water is directed upstream. It is possible that this water injection will influence the pitot pressure measurement if the probe tip encounters a subsonic region. However, because the data of the present work are to be compared to the fully expanded data of reference 12, which used the APL probe design, this probe design was used throughout the tests. The LaRC probes (fig. 4) were used to check the APL design accuracy. This design has several advantages. The most important advantage is that the cooling water is directed downstream and should not effect the pitot pressure measurement when the probe tip encounters a subsonic region. Other advantages are a small tip angle that can be used at lower Mach number without tip shock detachment and a smaller orifice diameter giving more point-like pitot pressure measurements required in regions of step gradients.

Pitot-pressure profiles were obtained with a single moving probe which was driven perpendicularly across the flow field at a rate of approximately 0.5 cm/sec. Comparisons of pitot pressures taken at the same points with the probe moving and stationary indicated that response of the pressure transducer was sufficient to give accurate measurements. In addition, over the range of test conditions investigated, probes of either design gave the same results for identical test conditions.

Photographs and Shadowgraphs

Black and white movies and shadowgraph pictures were taken of the flow field. The movies, taken at a frame rate that varied from 20 to 64 frames/sec, were used to check the pitot probe alignment and vibration. The shadowgraphs, taken at a constant frame rate of 24 frames/sec, were used to define the flow quality and are quite valuable for analyzing the flow field. Photographic records of both types were obtained on 16mm black and white movie film with an ASA number of 400 (DIN number of 27).

RESULTS AND DISCUSSIONS

Shadowgraphs

Referring to the shadowgraph of figure 5, the following details are apparent:

1. The injector extends downstream of the exit plane of the test stream nozzle.

2. There is a light area which outlines the facility nozzle test stream.

3. There is a light area at the center of the injector exit.

4. A shock wave appears attached to the injector lip.

5. The mixing boundary of the hydrogen jet is visible.

6. A shock wave appears to originate inside the jet and pass through the jet boundary several jet diameters downstream of the injector exit.

Details 1 and 2 orient the reader. Detail number 3 is an indication of the expansion that is expected since $p_j \approx 2\ p_\infty$. Detail number 4 is a shock wave whose exact starting location is not ascertainable from the shadowgraph of figure 5. Analytical considerations do not clarify its location, since there are several plausible explanations of what occurs in the base region of the injector lip. Each of the explanations results in slightly different starting locations for the shock wave.

The traditional interpretation given the base problem is pictured schematically in figure 6(a). This approach states that the flow from either side of the body expands into the base region, where a recirculation region is formed. The flow is then recompressed as the flows from either side meet. If the flow from one side of the body has a different flow angle or velocity than the other side, the resulting shock waves are not centered behind the body. The region downstream of the body is a wake region resulting from the shedding of the recirculation flow.

Another interpretation is that detail number 4 is an exit (underexpansion) shock caused by the compressive turning of the test stream as it encounters the bulge from the underexpanded jet as it expands into the test stream. Since $p_j \approx 2\ p_\infty$, the jet flow, which is at an angle of 5° at the injection exit, must further expand to an angle > 5°. The angle of the exit shock is such that the pressure rise across the shock produces a pressure equal to the pressure to which the jet expands. That is, the pressure behind the exit shock is exactly the pressure to which the jet expands at the injector lip. The resulting flow field is depicted in figure 6(b).

The actual situation is probably a combination of these two interpretations. Unfortunately, the shadowgraphs are not clear in the small base region area and the exact flow condition cannot be determined. However, it is informative to investigate the flow field which results from the two interpretations. For example, the expansion fans of figures 6(a) and 6(b) are due to different causes. The expansion fans in the traditional base problem interpretation are due to the finite thickness of the injector lip and disappear as the injector lip thickness approaches zero. On the other hand, the expansion fan in the exit shock interpretation is due to the underexpanded jet and does not disappear when the injector lip is infinitely thin.

The jet mixing boundary, described in detail 5, results from the fact that the velocity of the test stream flow behind the exit shock is different from that of the jet and because of the wake effects of the injector's lip. The second shock (detail 6), which originates inside the jet, also has two interpretations. If the traditional base problem interpretation of detail 4 is assumed, detail 6 is a recompression wave which is paired with detail 4. If the exit shock interpretation is used, detail 6 is an intersecting shock which lies along the last Mach line of the expansion fan issuing from the injector lip. Such an intersecting shock, as discussed in reference 20, is necessary

to eliminate an envelope singularity caused by the convergence of the Mach lines issuing from the jet boundary. In either case, the shock (detail 6) crosses the centerline and continues out to the mixing boundary where it is transmitted into the test stream. There is a reflected wave associated with the shock wave transmission at the mixing boundary (detail 5), whose type is determined by the criteria set forth in reference 21. In this reference, Kawamura defines a parameter

$$\Delta\lambda = \frac{1}{\gamma_j} \sin \mu_j \cos \mu_j - \frac{1}{\gamma_\infty} \sin \mu_\infty \cos \mu_\infty \qquad (1)$$

where γ is the specific heat ratio and μ the Mach angle. If the parameter $\Delta\lambda > 0$, then the wave reflected back into the jet is of the same type as the transmitted wave. If $\Delta\lambda < 0$, the reflected wave is of the opposite type. Of course, if $\Delta\lambda = 0$ there is no supersonic interface and thus no reflection occurs.

If viscosity is neglected and the traditional base region is assumed, the boundary becomes a simple jet boundary, and the injector's lip wake reduces to a recirculation region bounded by slip lines. The idealized jet flow pattern which illustrates these assumptions is shown in figure 6(c). If on the other hand, viscosity is neglected and the exit shock approach is assumed, the slip lines bounding the recirculation region do not coalesce to form a simple jet boundary. Instead, the slip lines are parallel and enclose a dead region as illustrated in figure 6(d).

If viscosity is included, both interpretations produce a flow field similar to that of figure 6(d), except the dead region and slip lines are replaced with a mixing region. The downstrean wave structure remains the same.

Pitot Pressure

Radial pitot pressure surveys were taken at several axial stations in the free-jet mode and at the end of the ducts when operating in the ducted mode. The pitot pressure data (surveys) for each mode of operation can be subdivided into reacting and nonreacting cases. In the reacting cases, the test stream is air and in the nonreacting cases the test stream is nitrogen.

Data for the free-jet reacting cases are presented in figure 7. The pitot surveys are, respectively, for axial locations of 0.318, 6.033, 9.525, 12.70, 17.78, and 25.4 cm. The nonreacting free-jet cases for the same axial locations as the reacting cases are presented in figure 8. The ducted reacting cases are presented in figure 9, and the ducted nonreacting cases are presented in figure 10. In each figure (figs. 7 through 10), the nondimensional pitot pressure is plotted against the nondimensional radial location. Pitot pressure is nondimensionalized by the corresponding test stream stagnation pressure. The radial location is nondimensionalized by the jet radius (r_j = 0.318 cm), and the zero location is the jet centerline.

The pitot pressures for both reacting and nonreacting mixtures exhibit conventional behavior in their spreading and decay of centerline pressures

except for their asymmetry. For the free-jet case in both reacting and nonreacting flows, the jets spread more on the right side than on the left side. (See figs. 7 and 8.) For the ducted reacting flows (fig. 9), the spreading is greater on the left side at the exit of two short ducts and greater on the right for the two longer ducts. Since rapid jet spreading and mixing is a major goal in the design of a scramjet combustor, considerable effort was devoted to finding the reason for this spreading. The hypothesis which provides the most reasonable answer is that it is due to the weak shock (labeled unbalanced wave), which is barely discernable on the right-hand side of figure 11 and for which no counterpart can be found on the left-hand side. This extraneous shock seems to originate inside the nozzle, intersects the jet mixing boundary, and is both reflected from and refracted through the boundary. One effect produced is a slightly different axial location of the intersections on opposite sides of the jet. If the asymmetry is produced by this extraneous shock, then it explains the fact that no asymmetrical spreading is observed in figures 7 and 8 at the farthest upstream station ($x = 1.0$), since this station is upstream of the point where the extraneous shock intersects the jet boundary. Also for the ducted case (fig. 9), the fact that the extraneous shock reflects from the duct walls would explain the reversal in sides on which spreading occurs when comparing results from the short and long ducts. The extraneous shock combines with the shock wave from within the jet and its reflected wave in a very localized region within the right-side mixing zone. The result of the intersection is a spreading of the mixing boundary that is not matched to the left of the centerline.

Later experience with the test stream nozzle indicates that the extraneous shock wave was probably caused by thermal buckling of the nozzle liner.

Comparison of free-jet and ducted profiles.- The pressure profiles for the free-jet and ducted configurations at $x = 30$ and 40 are compared in figure 12(a) for the reacting air-hydrogen stream, and in figure 12(b) for the nonreacting nitrogen-hydrogen flow. For the air-hydrogen jet, the comparison of free-jet and ducted flow (fig. 12(a)) indicates good agreement near the center region ($y = \pm 1$). However, a wide asymmetrical spreading of the flow to the left occurs with the ducted flow and a spreading to the right occurs in the free-jet. The extraneous wave previously discussed probably accounts for this behavior. For the nonreacting case (fig. 12(b)), the profiles are significantly flatter and more symmetrical. The ducted configuration is slightly less flat than the free-jet, but especially for the greater value of x, both profiles are flatter for the nonreacting flow than for reacting flow of figure 12(a). The original pitot pressure gradient has been spread over the flow field. The flatness suggests that mixing is more complete in the nonreacting flow than in reacting flow.

Comparison of reacting and nonreacting profiles.- In figures 13(a) and 13(b), the free-jet reacting data are compared with the nonreacting data for each of the axial locations. As can be seen in figure 13(a), the pitot profiles are quite similar at the smaller ($x = 1$, 19, and 30) locations. This is evidence of the fact that little reaction has occurred at these locations. The effect of reaction can be seen at the downstream locations. For example, the air-hydrogen surveys show that the internal boundary, defined by the location of the change in pressure from the lower mixing-region value to the free-stream value, remains well-defined at all locations. On the other hand, the

profiles for the nitrogen-hydrogen case are generally flatter. This is expected, since reaction tends to strongly affect the Mach number through the static temperature, and therefore directly affects the pitot pressure in the mixing-reacting zone. Of course, other differences may well be caused by the different manner in which shock and expansion waves interact with reacting and nonreacting mixing zones.

Static Pressure

When operating in the ducted mode, static pressure measurements were made at several axial locations along the ducts. The measured static pressures for the reacting and nonreacting cases are presented in figure 14. In this figure, the nondimensional static pressure is plotted against the nondimensional axial location.

Since the static pressure cases were taken simultaneously with the measurement of the radial pitot surveys at the end of the ducts, they have the same test conditions. For example, the pitot profile at the end of the 9.53 cm duct of figure 9 has the same test conditions as the static pressures presented in figure 14 for the 9.53 cm duct.

In general, the static pressure variation has the same trend for both the reacting and nonreacting cases. The amplitude of the sawtooth variations for the nonreacting case, however, is usually less than that for the reacting case. For both cases there is a general trend of increasing static pressure with downstream distance. The more rapid increase for the reacting case is expected since heat addition raises the pressure. The pressure rise for the nonreacting flow is due to the reflecting shock system only.

Comparison of fully expanded and underexpanded data.- In this section, pitot pressure data of the present work are compared with similar fully expanded jet data published in reference 12. Figures 15 and 16, respectively, give the centerline pitot pressures for the reacting and nonreacting cases at several axial locations. The circular symbols represent the fully expanded data from reference 12, and the square symbols underexpanded data from the present work. The solid curves are the theoretical values presented in reference 12 for the fully expanded case. Note that in both the reacting and nonreacting flows, the high centerline exit pressure of the underexpanded case rapidly decays to approximately the fully expanded case at $x = 20$, dips below the fully expanded case at $x = 56$, and rises above the fully expanded case at $x = 80$. At the $x = 80$ location, the reacting underexpanded case is approximately 30 percent greater than the fully expanded case and approximately 4 percent greater in the nonreacting cases. The stronger shock and reflected wave structure for the underexpanded case probably produce these effects. This suggests that the wave structure is important even at downstream locations, and therefore must be included in any further analysis of the underexpanded case. Complete profile comparisons for this station are given in figures 17 and 18. The comparisons indicated at the centerline are seen to extend throughout the transverse plane in each case.

CONCLUDING REMARKS

This investigation furnishes experimental data on the mixing of an underexpanded hydrogen jet in supersonic flow. The reacting and nonreacting data are for a Mach 2 test stream of air or nitrogen, and a Mach 2 hydrogen jet whose exit pressure is approximately twice the test stream static pressure. The investigation was conducted in both a free-jet configuration and a ducted configuration, and furnished data for four different duct lengths.

The pressure profiles for the nitrogen-hydrogen (nonreacting) flow are flatter than the profiles for the air-hydrogen (reacting) flow. Ducting the flow had little effect on the pressure near the centerline. However, asymmetries present in the air-hydrogen flow were reflected by the duct and appeared on the opposite side as compared to the free-jet flow. Ducting produced a distinct near-centerline region of low pitot pressure for the reacting case. Heat release in the ducted flow caused a more rapid increase in the static pressure with downstream distance than occurs for the ducted nonreacting flow.

Comparison of pitot pressure profiles for the underexpanded jet with experimental and theoretical results for a fully expanded jet indicate that the additional waves introduced by the underexpansion are still very evident even at far downstream locations.

REFERENCES

1. Ferri, A.: Review of Scramjet Propulsion Technology. J. Aircraft, vol. 5, no. 1, Jan.-Feb. 1968, p. 3.

2. Henry, J. R.; and Beach, H. L.: Hypersonic Air-Breathing Propulsion Systems. NASA SP-292, Nov. 1971.

3. Henry, J. R.; and Anderson, G. Y.: Design Considerations for the Airframe-Integrated Scramjet. Presented at the First International Symposium for Air-Breathing Engines (Marseille, France), June 1972.

4. Becker, J. V.: New Approaches to Hypersonic Aircraft. Paper presented at Seventh Congress of International Council of the Aeronautical Sciences (Rome, Italy), Sept. 1970.

5. Trexler, C. A.: An Experimental Investigation of the Forebody of a Hypersonic Inlet Model and a Comparison with Theory. M.S. Thesis, Va. Polytech. Inst. and State Univ., April 1972.

6. Trexler, C. A.: Performance of an Inlet for an Integrated Scramjet Concept. J. Aircraft, vol. 11, no. 9, Sept. 1974, pp. 589-591.

7. Edwards, C. L. W.: A Forebody Design Technique for Highly Integrated Bottom-Mounted Scramjets with Application to a Hypersonic Research Airplane. NASA TN D-8369, Dec. 1976.

8. Small, W. J.; Weidner, J. P.; and Johnston, P. J.: Scramjet Nozzle Design and Analysis as Applies to a Highly Integrated Research Airplane. NASA TM X- 71972, Nov. 1974.

9. Pinckney, S. Z.: Turbulent Heat-Transfer Prediction Method Fan Application to Scramjet Engines. NASA TN D-7810, Nov. 1974.

10. Cohen, L. S.; and Guile, R. N.: Investigation of the Mixing and Combustion of Turbulent, Compressible Free Jets. NASA CR-1473, Dec. 1969.

11. Eggers, J. M.: Turbulent Mixing of Coaxial Compressible Hydrogen-Air Jets. NASA TN D-6487, Sept. 1971.

12. Beach, H. L.: Supersonic Mixing and Combustion of a Hydrogen Jet in a Coaxial High-Temperature Test Gas. Presented at the AIAA/SAE Eighth Propulsion Joint Specialist Conference (New Orleans, Louisiana), Nov.-Dec. 1972.

13. Casaccia, A.; and Rupp, R. L.: A Supersonic Combustion Test Program Utilizing Gas Sampling, Optical and Photographic Measuring Techniques. NASA CR-66393, July 1967.

14. Rogers, R. C.; and Eggers, J. M.: Supersonic Combustion of Hydrogen Injected Perpendicular to a Ducted Vitiated Airstream. Presented at the AIAA/SAE Ninth Propulsion Conference (Las Vegas, Nevada), Nov. 1973. (AIAA Paper No. 73-13222.)

15. Staff of Langley Research Center and AiResearch Manufacturing Co., The Garrett Corp.: Hypersonic Research Engine Project Technological Status 1971. NASA TM X-2572, Sept. 1971. (Declassified 12/11/74.)

16. Wieting, A. R.; and Guy, R. W.: Preliminary Thermal-Structural Design and Analysis of an Airframe Integrated Hydrogen-Cooled Scramjet. Paper presented at the AIAA 13th Aerospace Sciences Meeting (Pasadena, Calif.), Jan, 1975.

17. Dash, S.; and DelGuidice, P.: Analysis of Supersonic Combustion Flow Fields with Embedded Supersonic Regions. NASA CR-112223, Nov. 1972.

18. Kalben, P.: A Fortran Program for the Analysis of Supersonic Combustion Flow Fields with Embedded Supersonic Regions. Advanced Technology Laboratories, Inc., Report TM 167.

19. Trout, O. F.: Design, Operation and Testing Capabilities of the Langley 11-Inch Ceramic-Heated Tunnel. NASA TN D-1598, Feb. 1963.

20. Courant, R.; and Friedrichs, K. O.: Flow in Nozzles and Jets. Supersonic Flow and Shock Waves. Chapter V. Interscience Publisher, Inc., New York, 1948.

21. Kawamura, Ryuma: Reflection of a Wave at an Interface of Supersonic Flows and Wave Patterns in a Supersonic Compound Jet. Journal of the Physical Society of Japan, vol. 5, no. 5, Sept.-Oct. 1952, pp. 482-485.

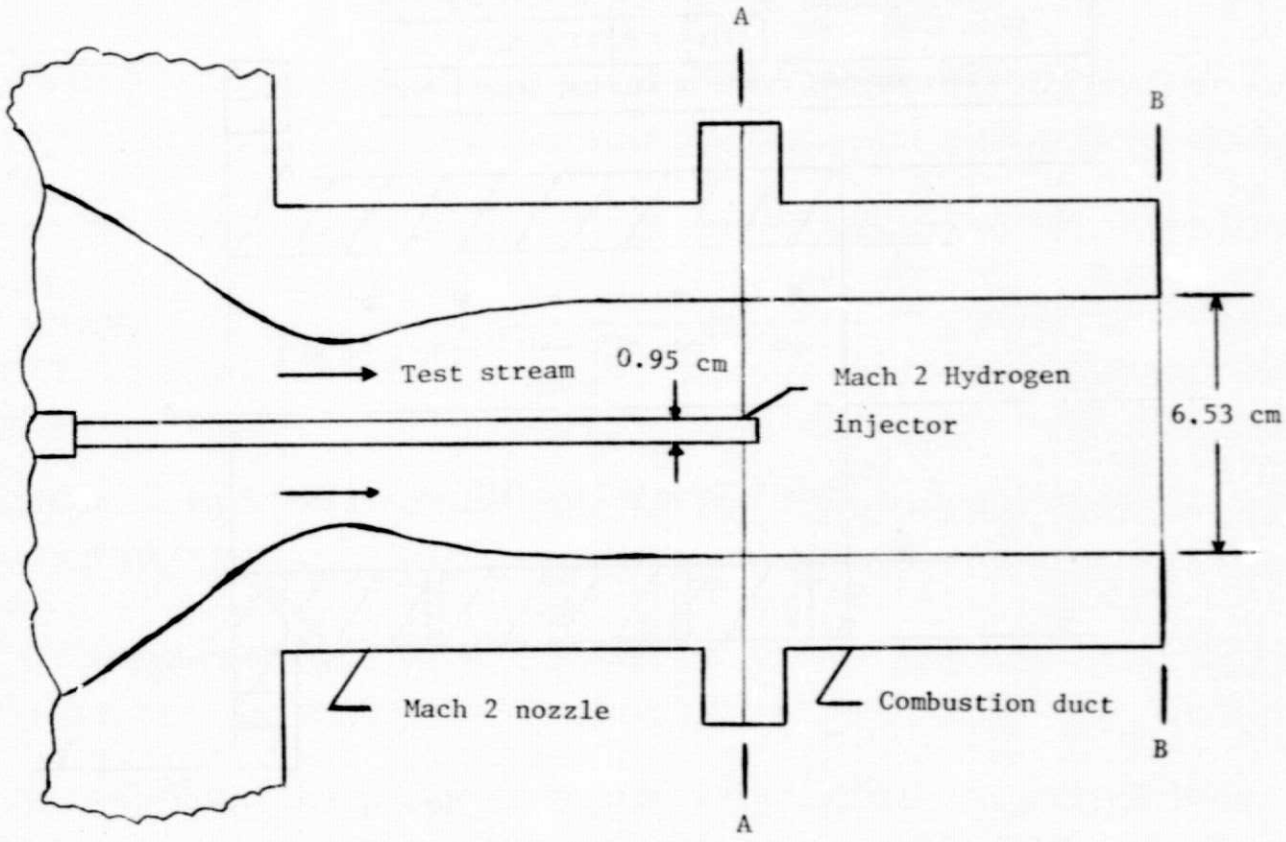

Figure 1.- Schematic of the coaxial supersonic combustion apparatus.

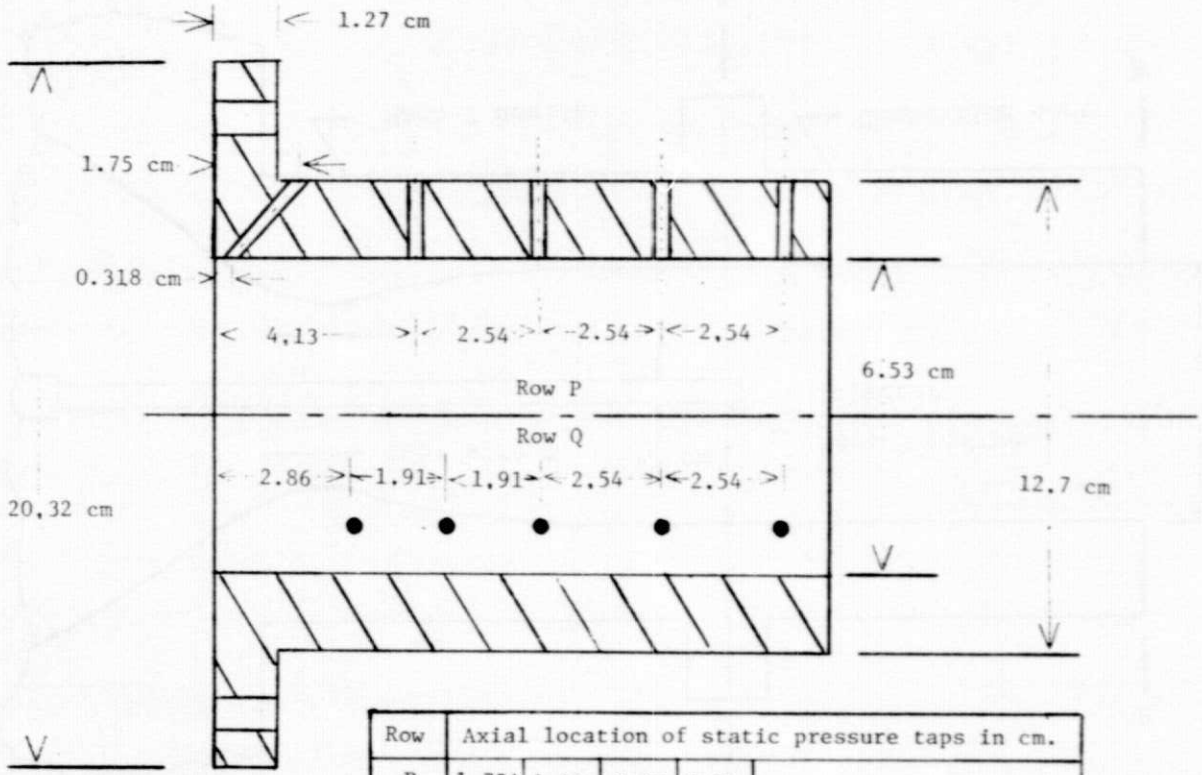

Row	Axial location of static pressure taps in cm.				
P	1.75*	4.13	6.67	9.21	Spaced at 2.54 cm intervals from previous locations to the duct exit.
Q	2.86	4.76	6.67	9.21	
R	3.49	5.40	-	9.21	

*This tap drilled at an angle so that it opens into the duct at an axial location of 0.3175 cm.

Figure 2.- Half section of 12.7 cm length duct (taken in the plane bisecting the pressure taps of Row P) with axial locations for all four ducts.

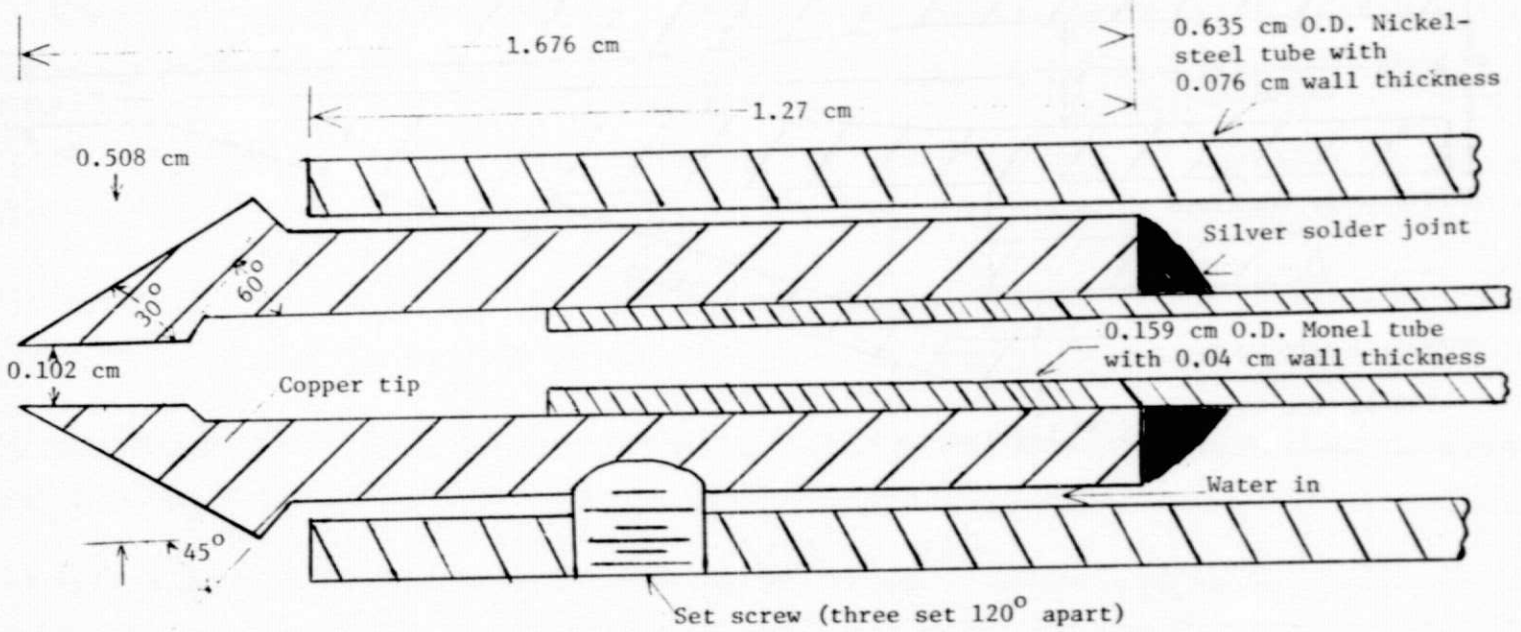

Figure 3.- Cross section of the modified Johns Hopkins' probe (APL).

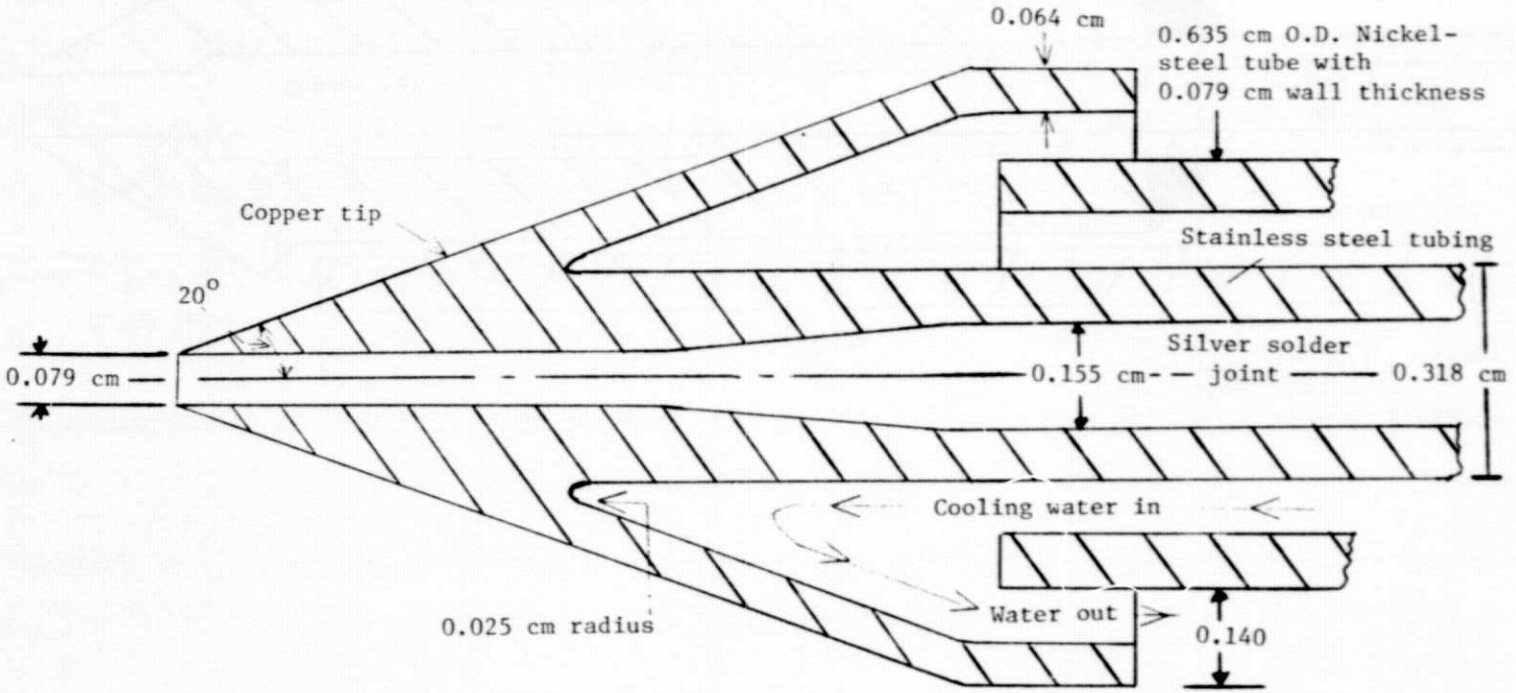

Figure 4.- Half-section of the LRC probe.

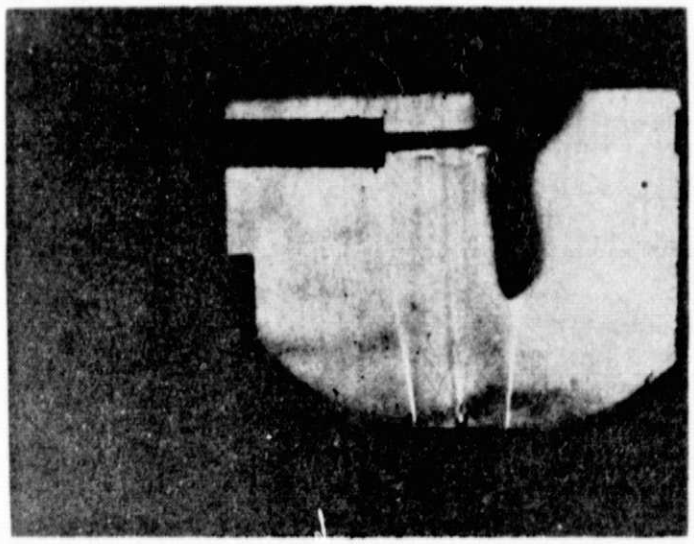

(a) Test stream and jet.

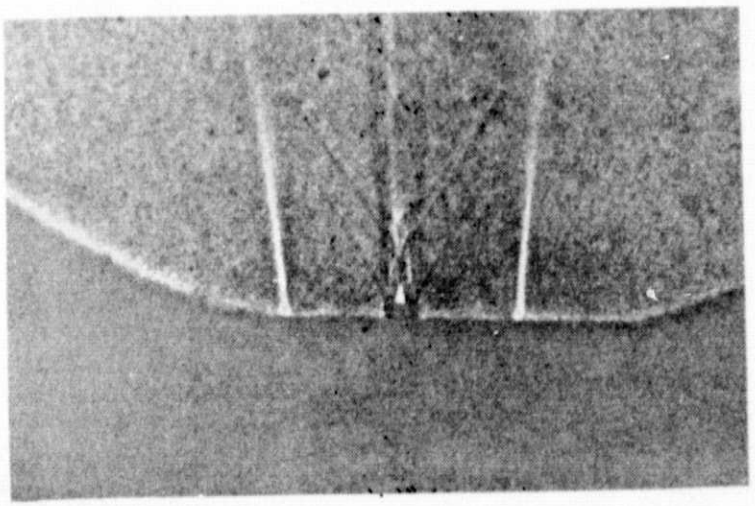

(b) Blow-up of wave structure.

Figure 5. - Shadowgraph of the test stream and jet in the free-jet mode with combustion.

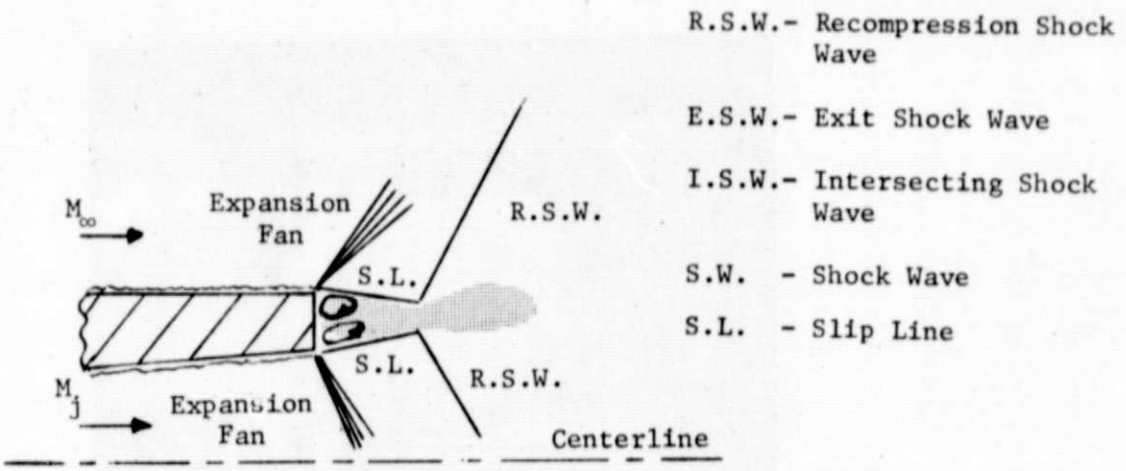

(a) Traditional schematic of the base region with recompression, and wake.

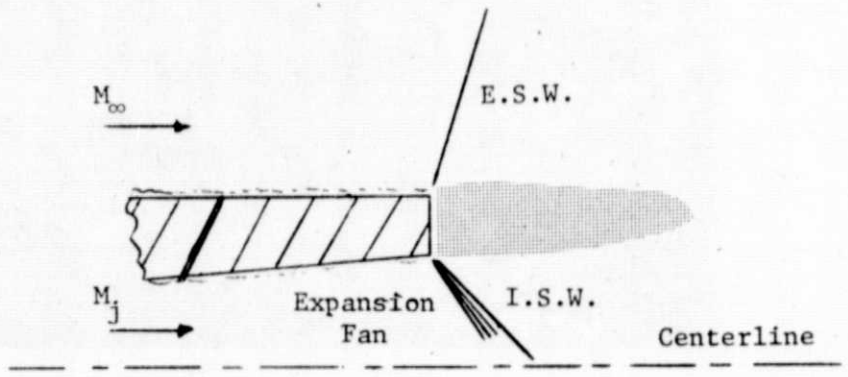

(b) Schematic of the base region when an exit shock is assumed.

Figure 6.- Flow field schematics.

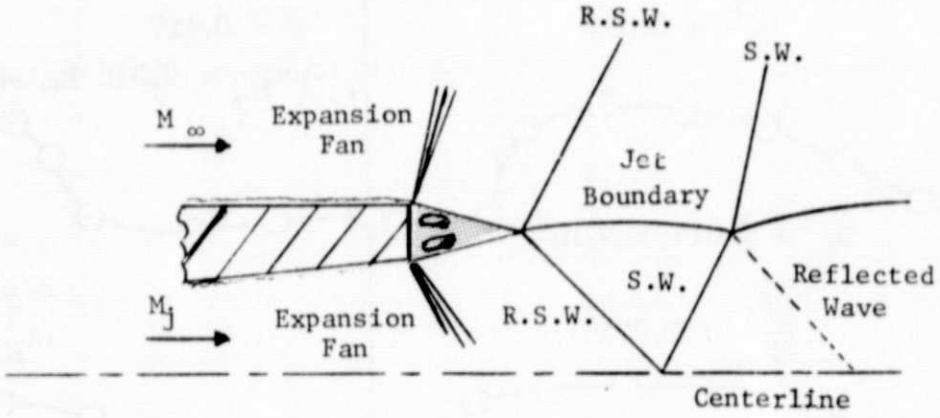

(c) Idealized schematic of the test stream-jet interaction (traditional).

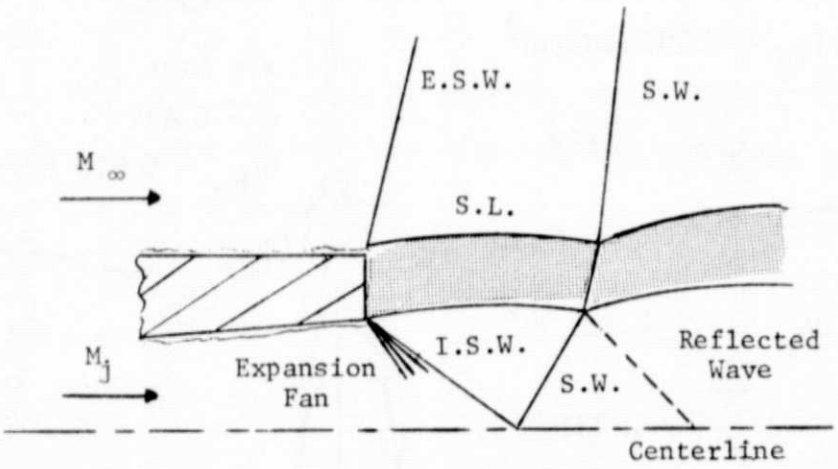

(d) Idealized schematic of the test stream-jet interaction (exit shock).

Figure 6. - Conclude.

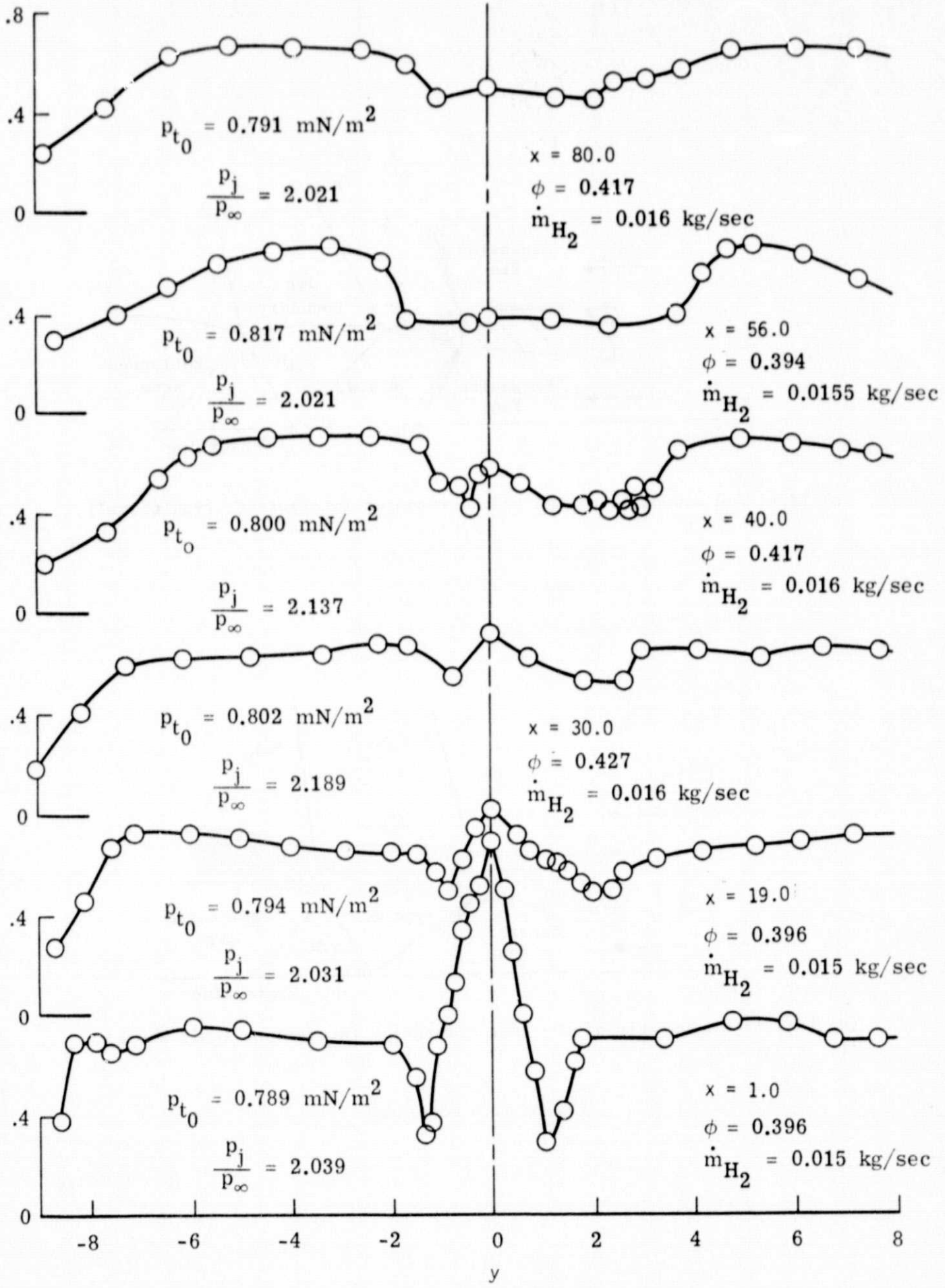

Figure 7.- Lateral pitot pressure distributions in an reacting free jet at varying downstream locations.

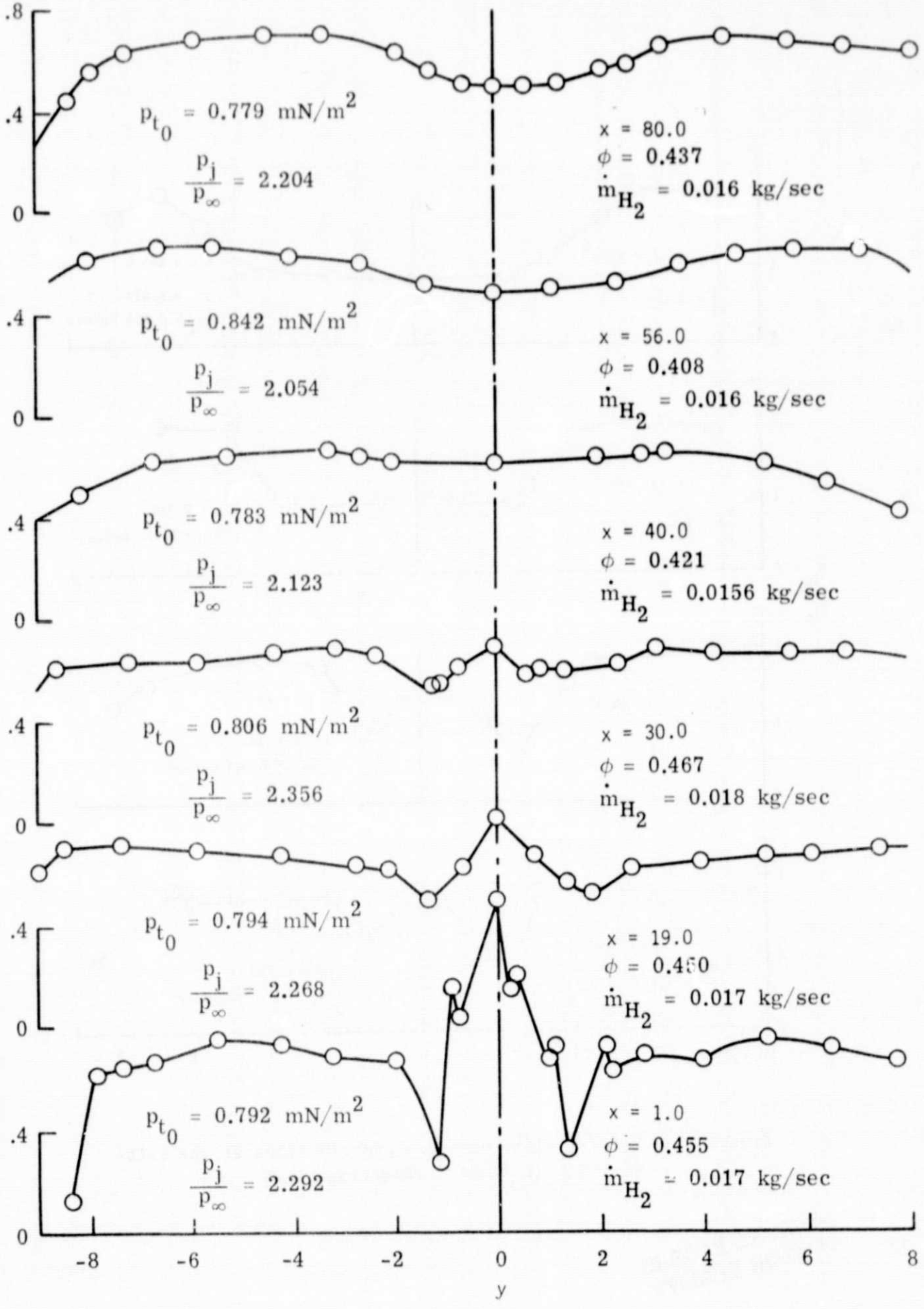

Figure 8.- Lateral pitot pressure distributions in a nonreacting free jet at varying downstream locations.

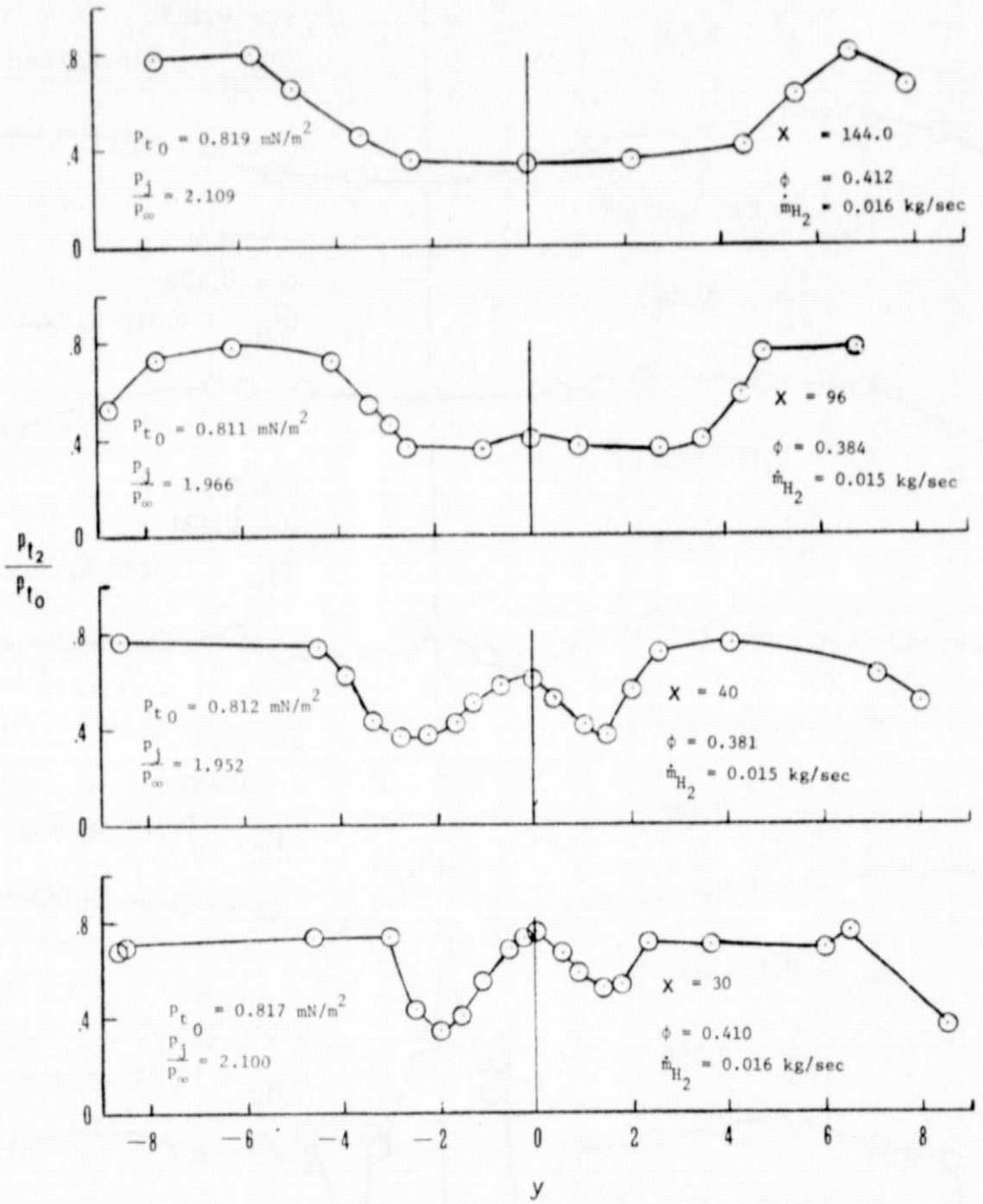

Figure 9. - Lateral pitot pressure distributions at the exits of the four ducts. (Reacting Flow)

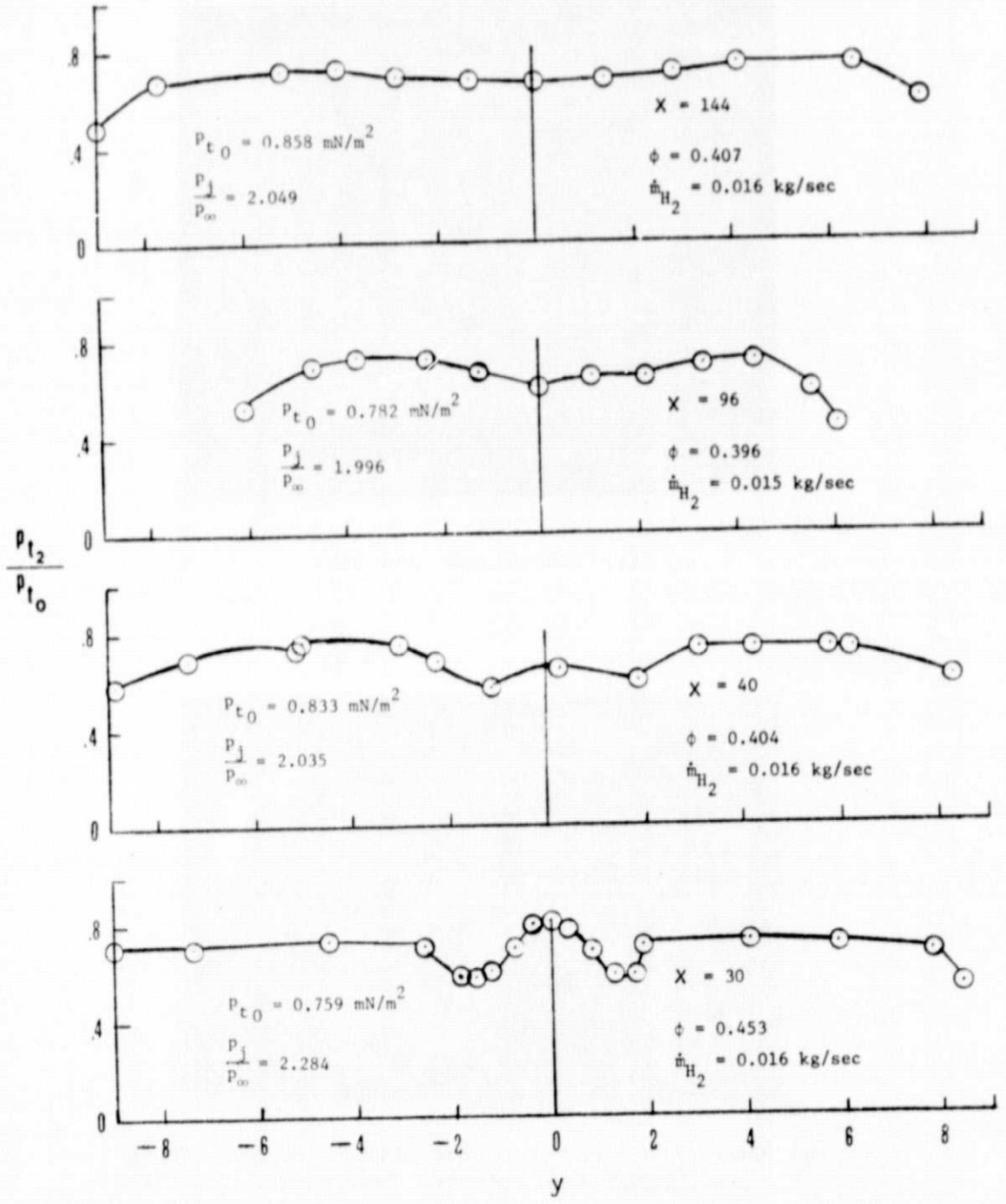

Figure 10.- Lateral pitot pressure distributions at the exits of the four ducts. (Nonreacting Flow)

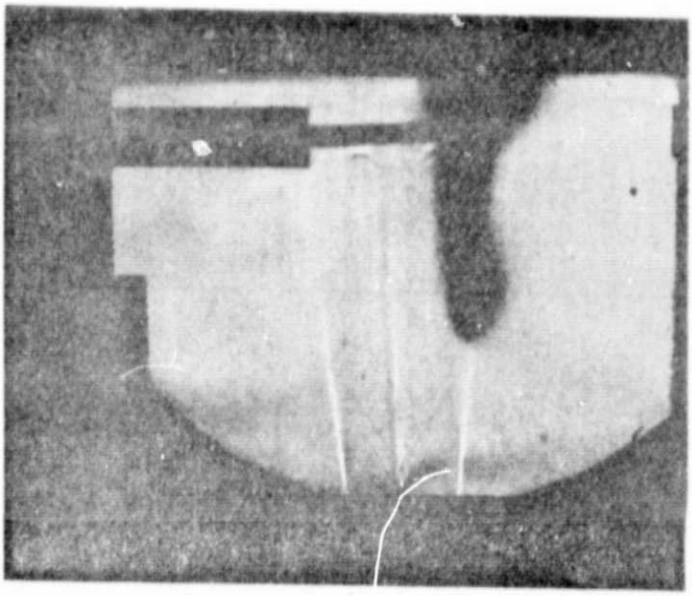

(a) Test stream and jet.

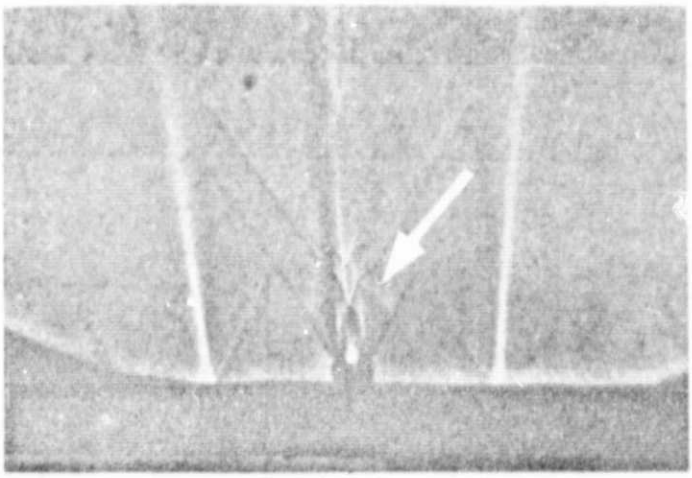

(b) Blow-up of wave structure with arrow indicating unbalanced wave entering from right.

Figure 11. - Shadowgraph showing additional wave structure to the right of the centerline which may account for the nonsymmetrical flow activity.

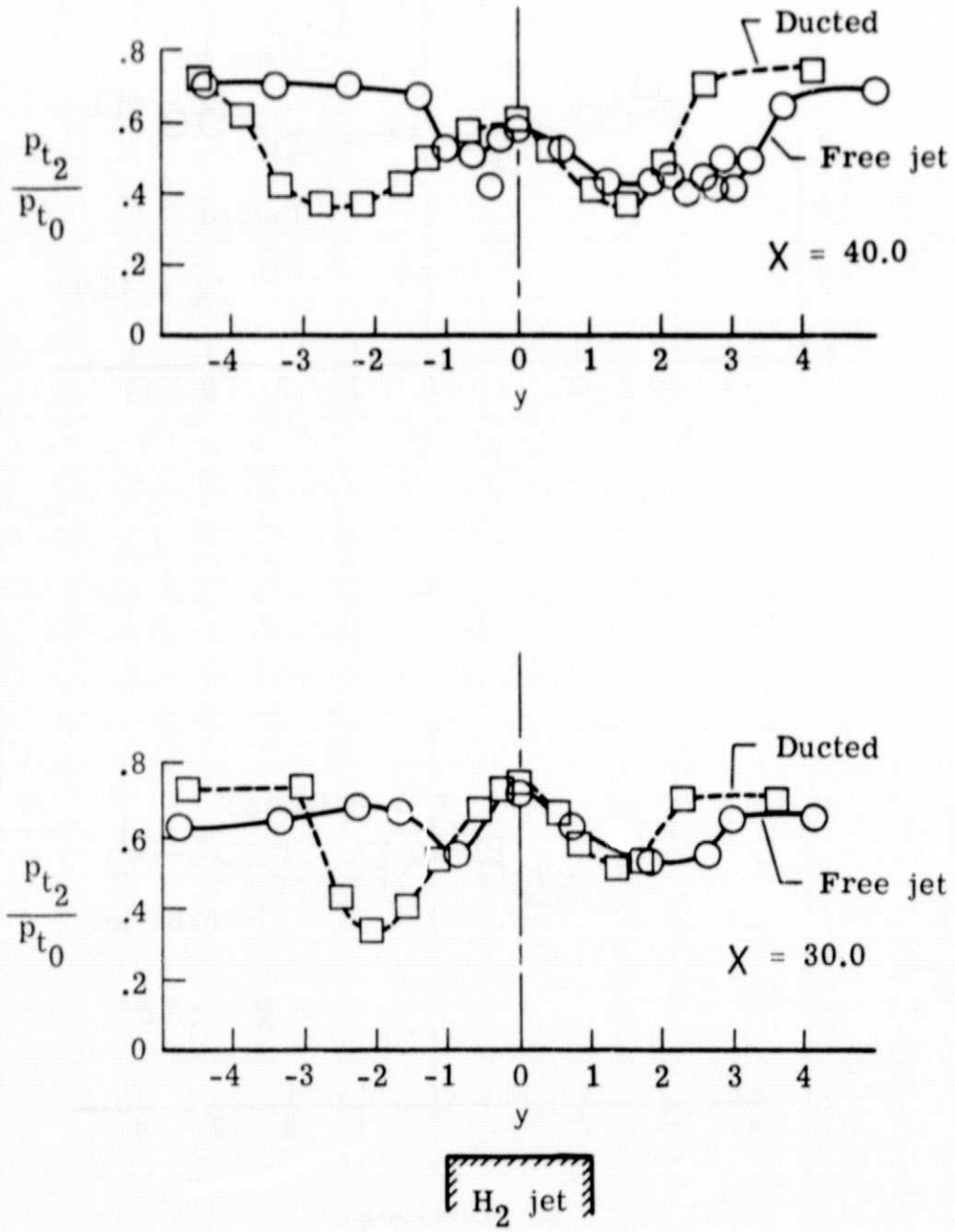

(a) Hydrogen-air (reacting).

Figure 12.- Comparison of ducted and free jet results.

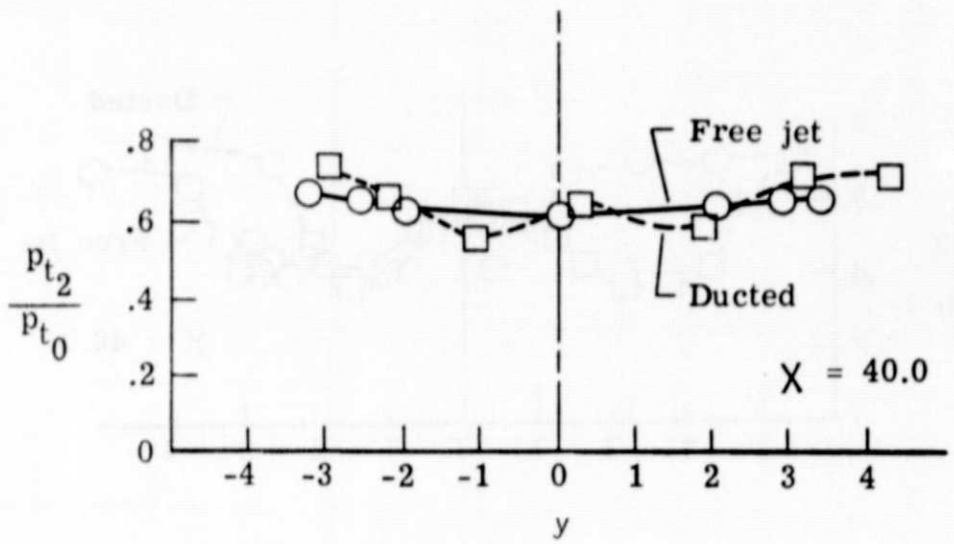

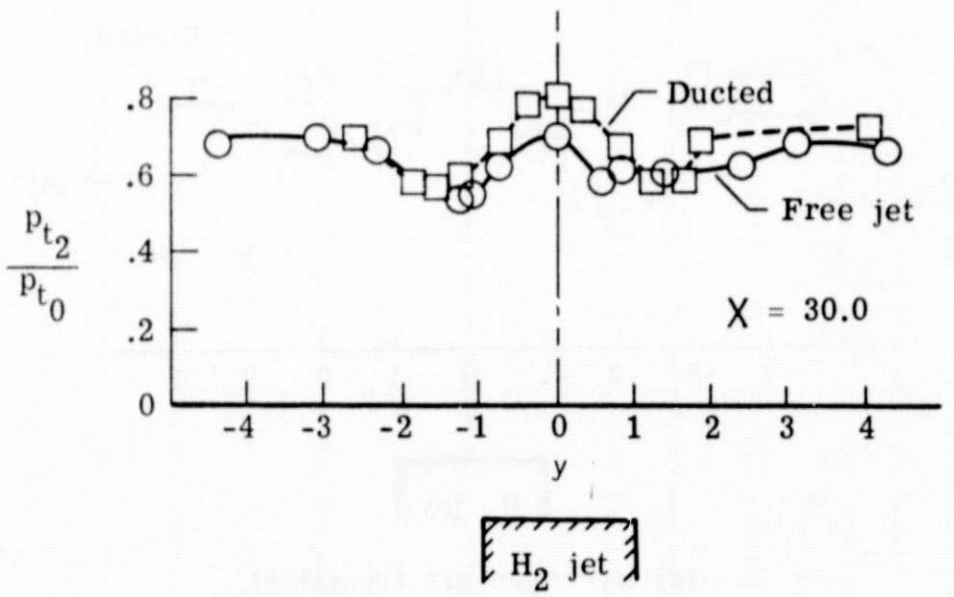

(b) Hydrogen-nitrogen (nonreacting).

Figure 12.- Concluded.

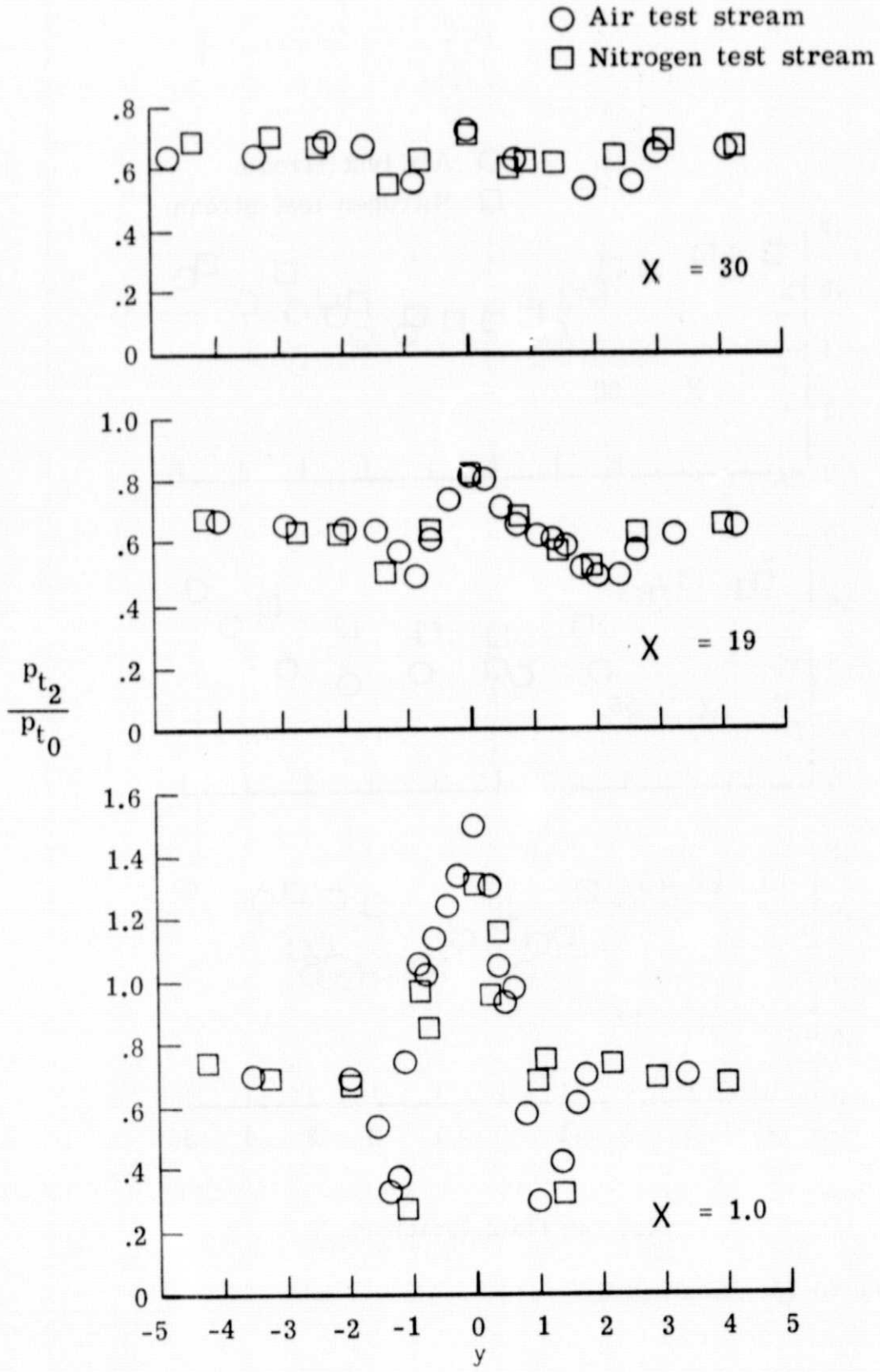

(a) Near field locations.

Figure 13.- Comparison of the reacting and nonreacting free-jet cases.

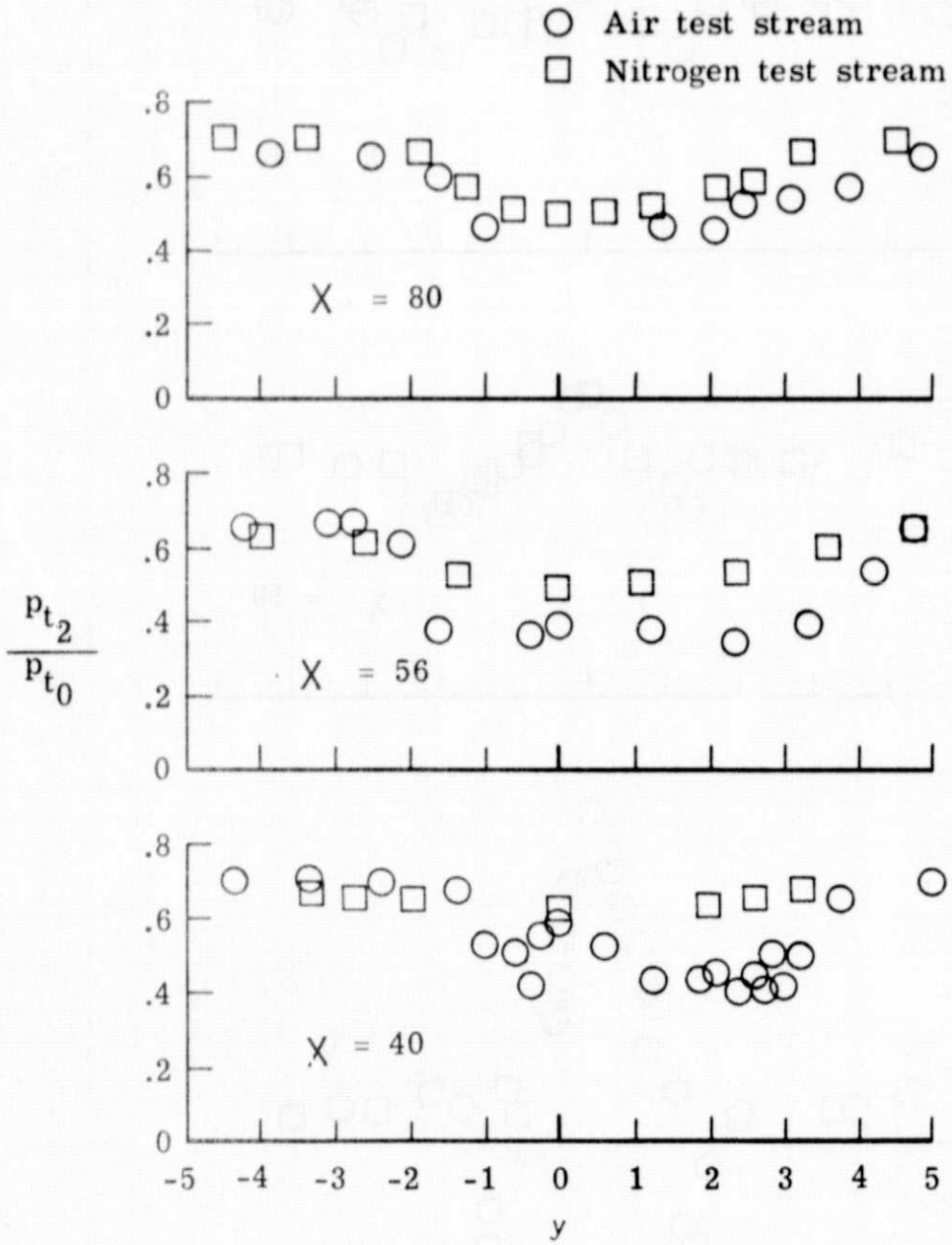

(b) Far field locations.

Figure 13.- Concluded.

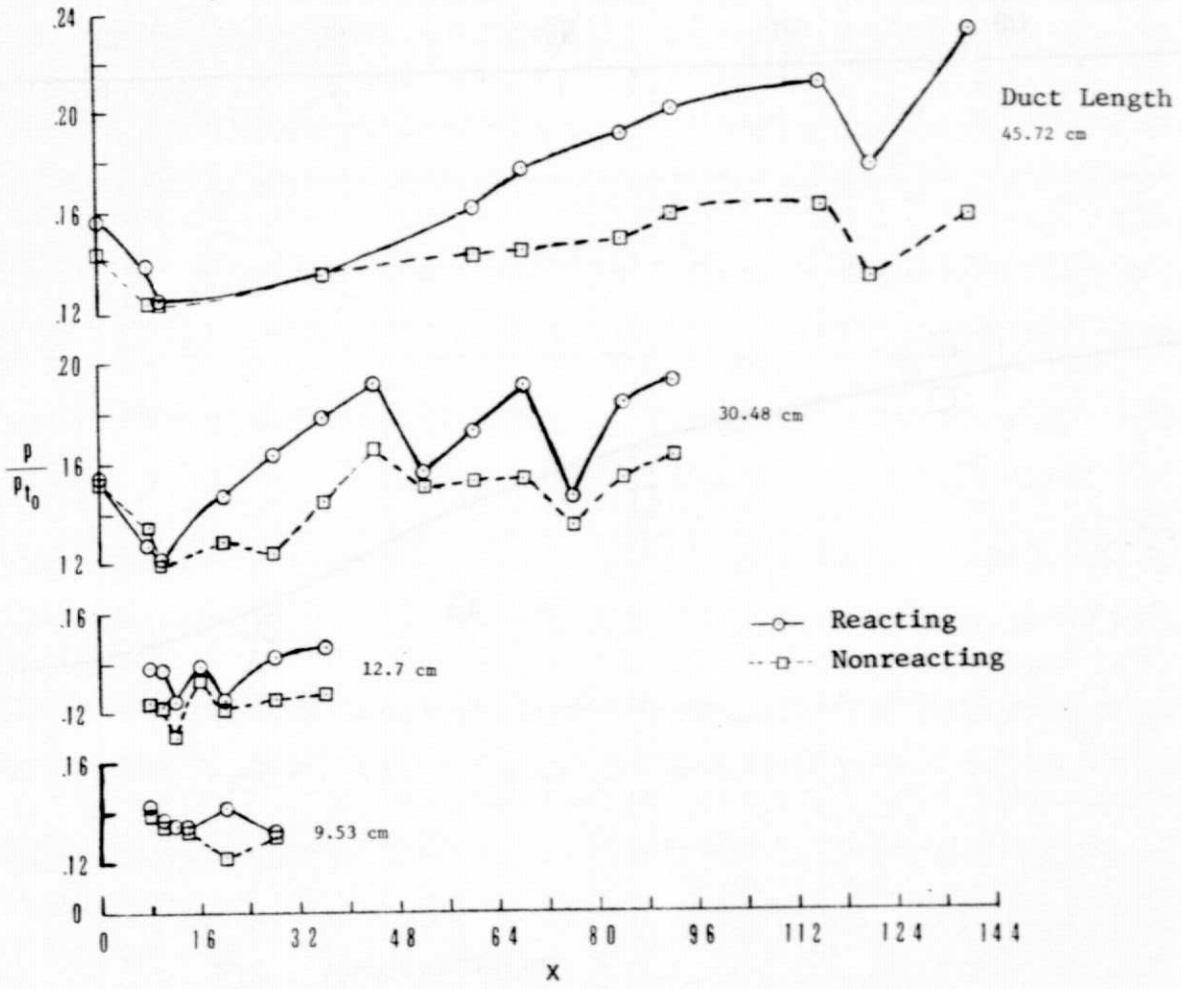

Figure 14.- Static pressures along the duct wall.

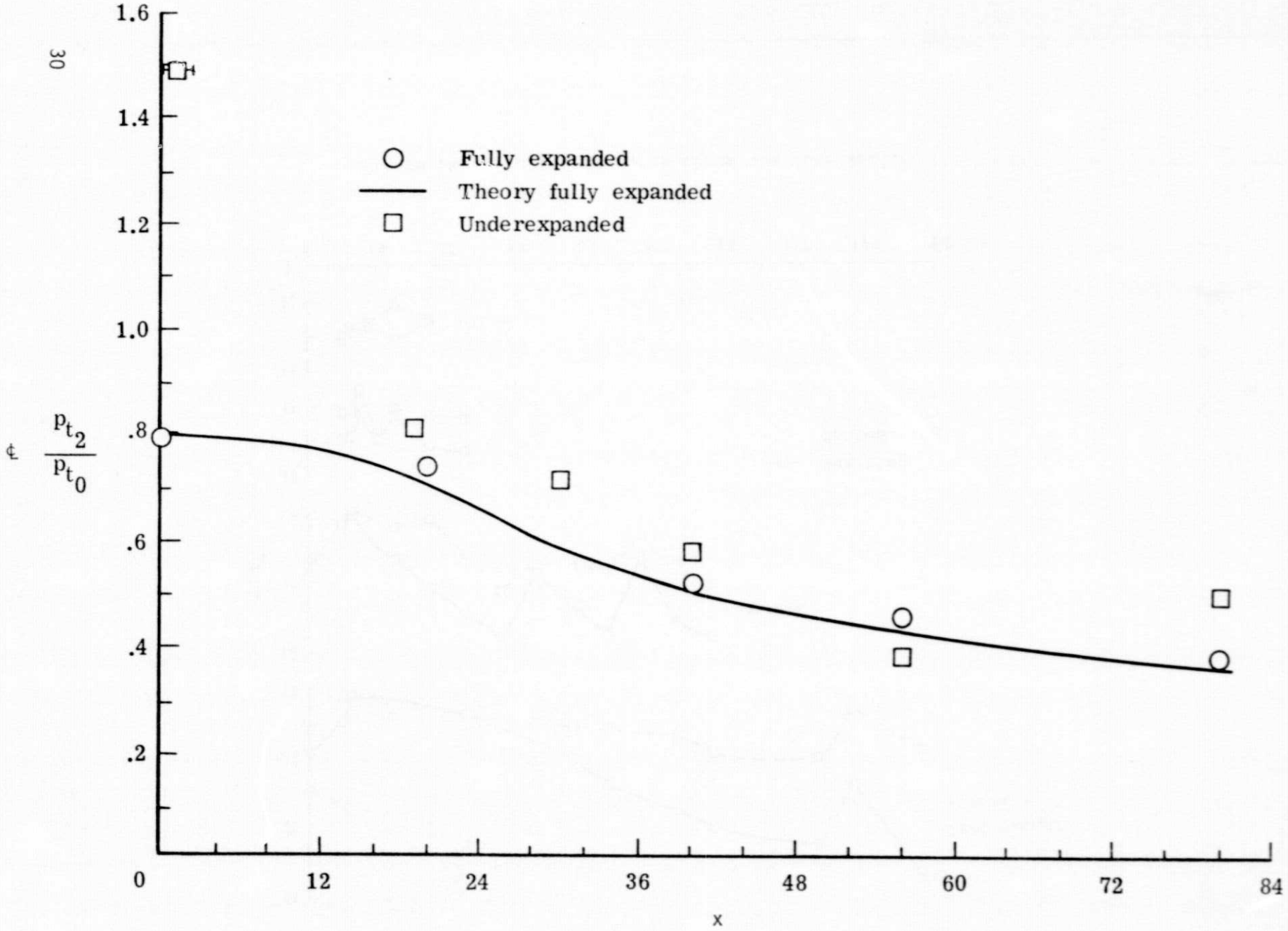

Figure 15.- Center-line decay of pitot pressure. (Reacting flow)

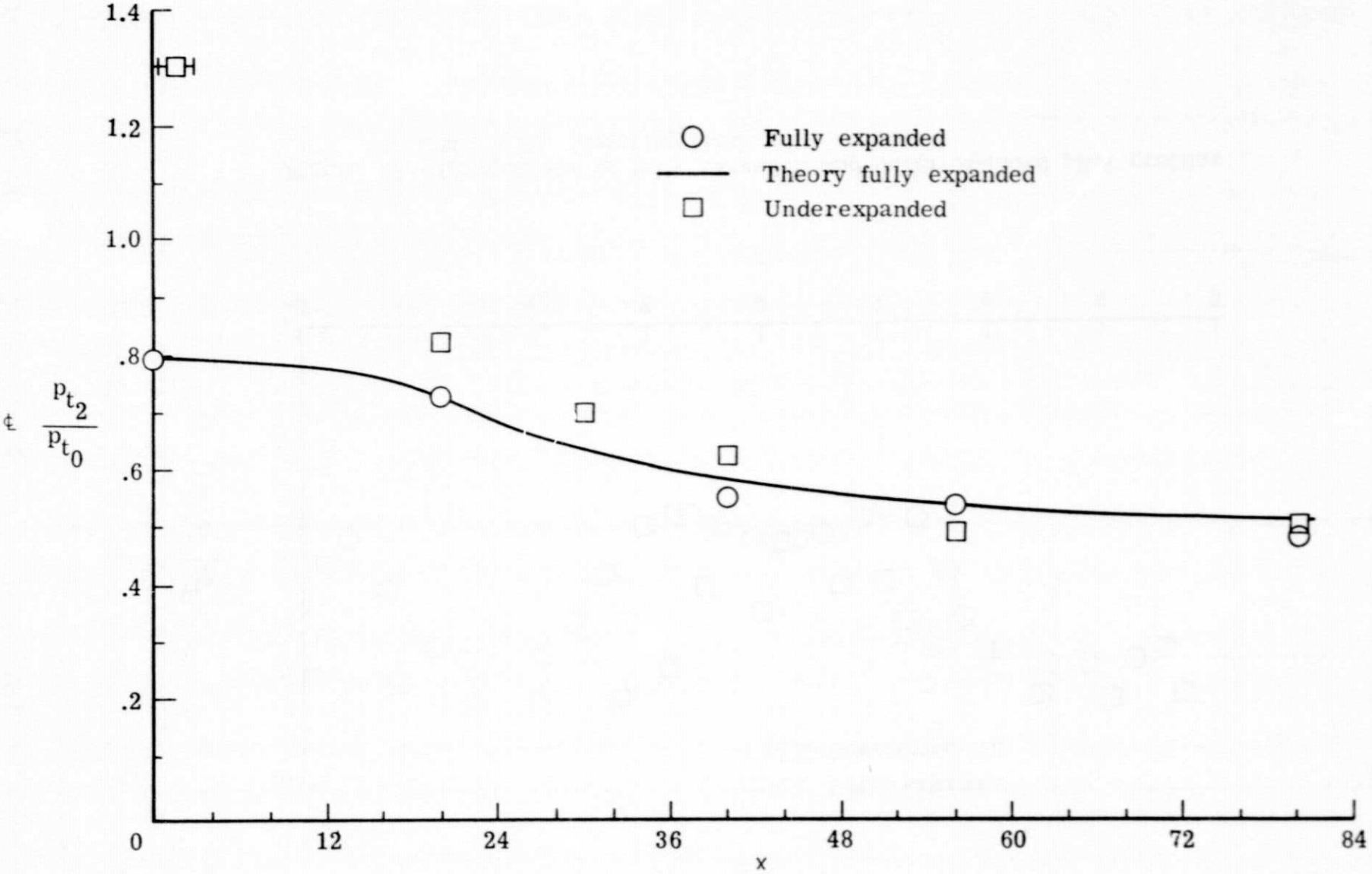

Figure 16.- Center-line decay of pitot pressure. (Nonreacting flow)

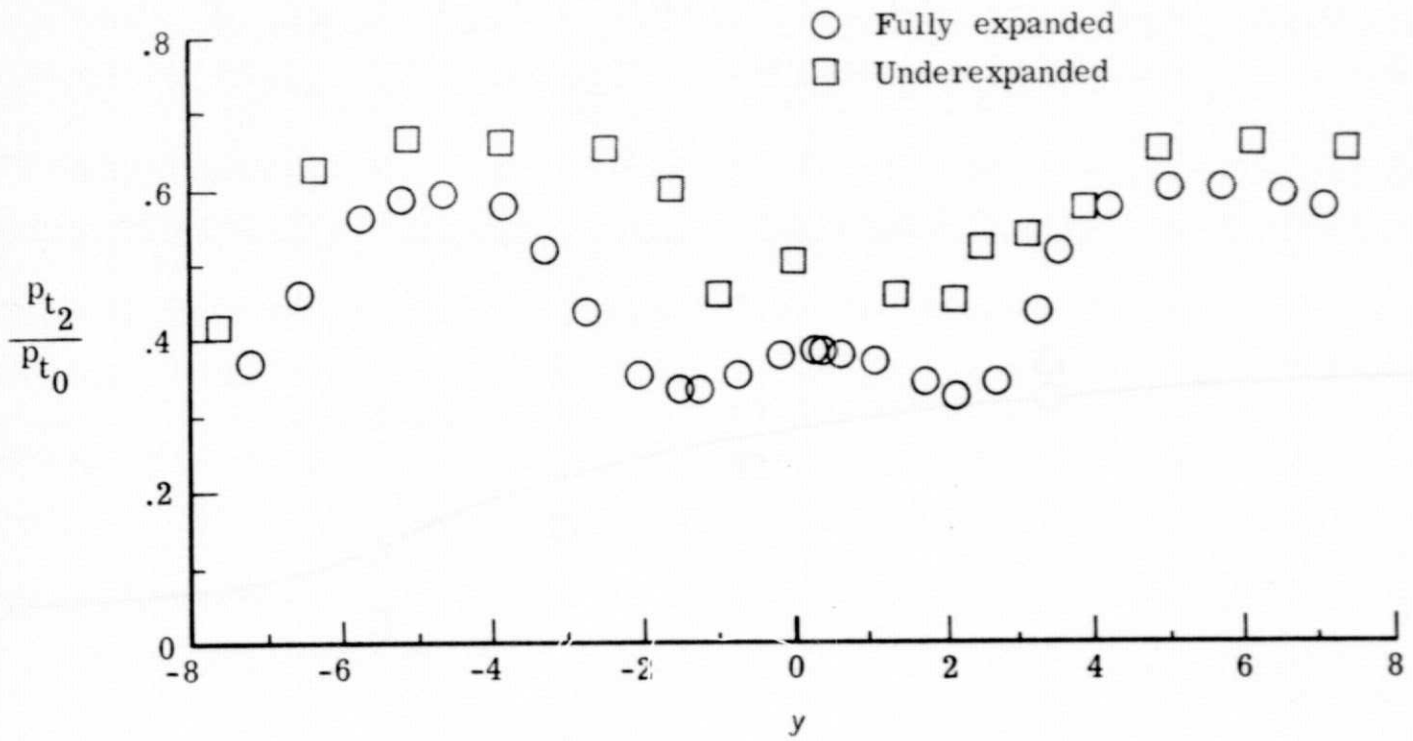

Figure 17.- Comparison of fully expanded and underexpanded pitot profiles at x = 80. (Reacting flow)

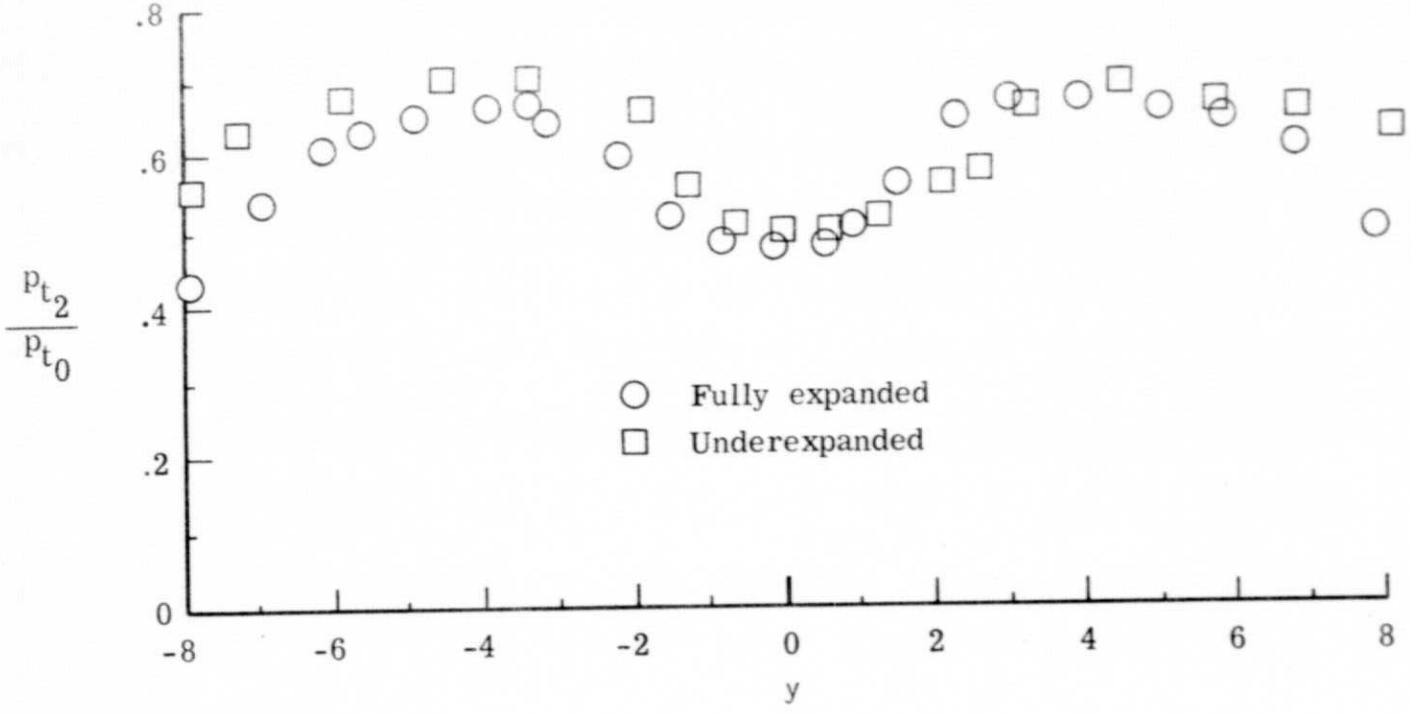

Figure 18.- Comparison of fully expanded and underexpanded pitot profiles at x = 80. (Nonreacting flow)